Supplementary Information

Deep learning enables fast, gentle STED microscopy

Vahid Ebrahimi[1], Till Stephan[2,8], Jiah Kim[3], Pablo Carravilla[4,5], Christian Eggeling[4,5,6,7], Stefan Jakobs[2,8,9], Kyu Young Han[1,*]

[1]CREOL, The College of Optics and Photonics, University of Central Florida, Orlando, FL, USA

[2]Department of NanoBiophotonics, Max Planck Institute for Multidisciplinary Sciences, Göttingen, Germany

[3]Department of Cell and Developmental Biology, University of Illinois at Urbana-Champaign, Urbana, IL, USA

[4]Leibniz Institute of Photonic Technology e.V., Jena, Germany, member of the Leibniz Centre for Photonics in Infection Research (LPI), Jena, Germany

[5]Faculty of Physics and Astronomy, Institute of Applied Optics and Biophysics, Friedrich Schiller University Jena, Jena, Germany

[6]Jena School for Microbial Communication, Friedrich Schiller University Jena, Jena, Germany

[7]Medical Research Council Human Immunology Unit, Weatherall Institute of Molecular Medicine, University of Oxford, Oxford, United Kingdom

[8]Department of Neurology, University Medical Center Göttingen, Göttingen, Germany

[9]Translational Neuroinflammation and Automated Microscopy, Fraunhofer Institute for Translational Medicine and Pharmacology ITMP, Göttingen, Germany

*Correspondence to Kyu Young Han: kyhan@creol.ucf.edu

Supplementary Videos

Supplementary video 1. Time-lapse STED imaging of mitochondria dynamics with a pixel time of 90 µs. HeLa cells were labeled with PK Mito Orange.

Supplementary video 2. Fast deep-learning STED imaging of mitochondria dynamics with a pixel time of 1 µs. HeLa cells were labeled with PK Mito Orange.

Supplementary video 3. Two-color live-cell deep-learning STED imaging of mitochondria (green) and ER (magenta) in HeLa cells with a pixel time of 1 µs. Mitochondria was labeled with PK Mito Orange, and ER was labeled with SiR-Halo.

Supplementary video 4. Deep-learning live-cell STED imaging with deconvolution. COS-7 cells were labeled with PK Mito Orange.

Supplementary video 5. Denoising fast 3D STED *xz* imaging of giant unilamellar vesicles (GUV) labeled with NR4A with a pixel time of 2 µs.

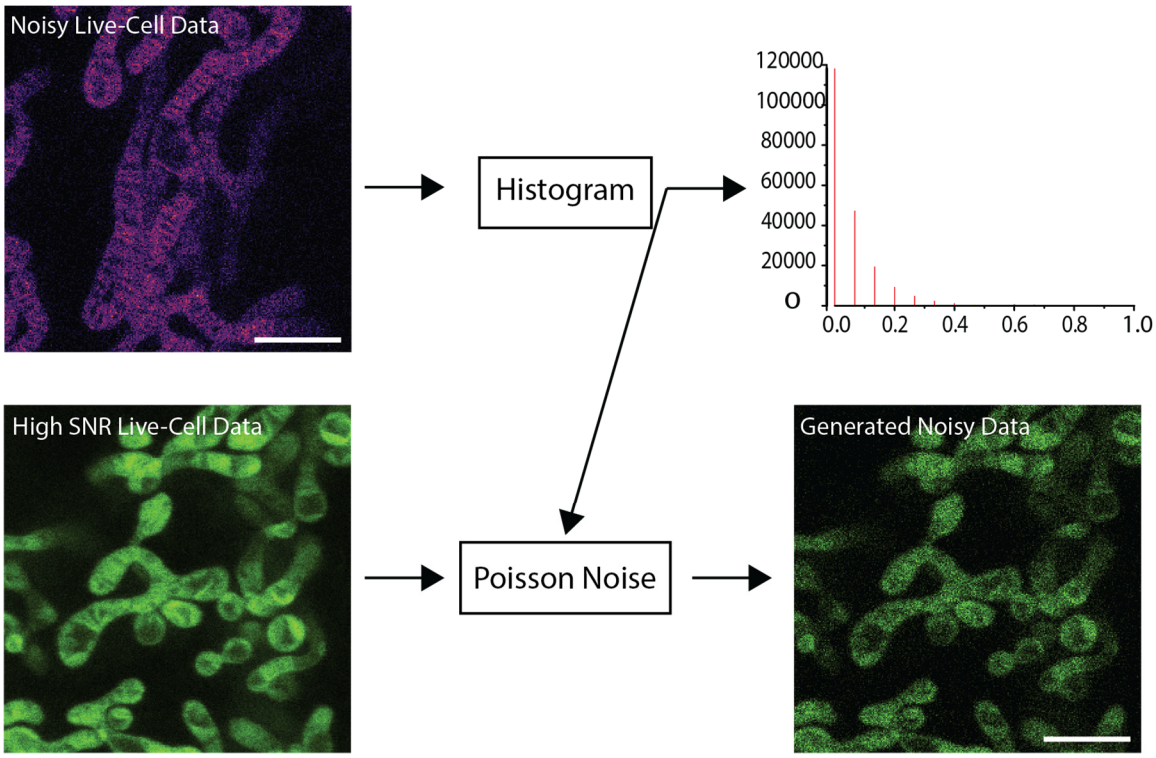

Supplementary Fig. 1, Semi-synthetic dataset generation. Poisson noise was applied to the high SNR STED images of cristae labeled with PK Mito Orange in HeLa cells to generate a pair of noisy and high SNR data for training UNet-RCAN. The amount of Poisson noise was adjusted such that the intensity histogram of the generated noisy data resembles that of the noisy live cell STED data (See Methods). Scale bars, 2μm.

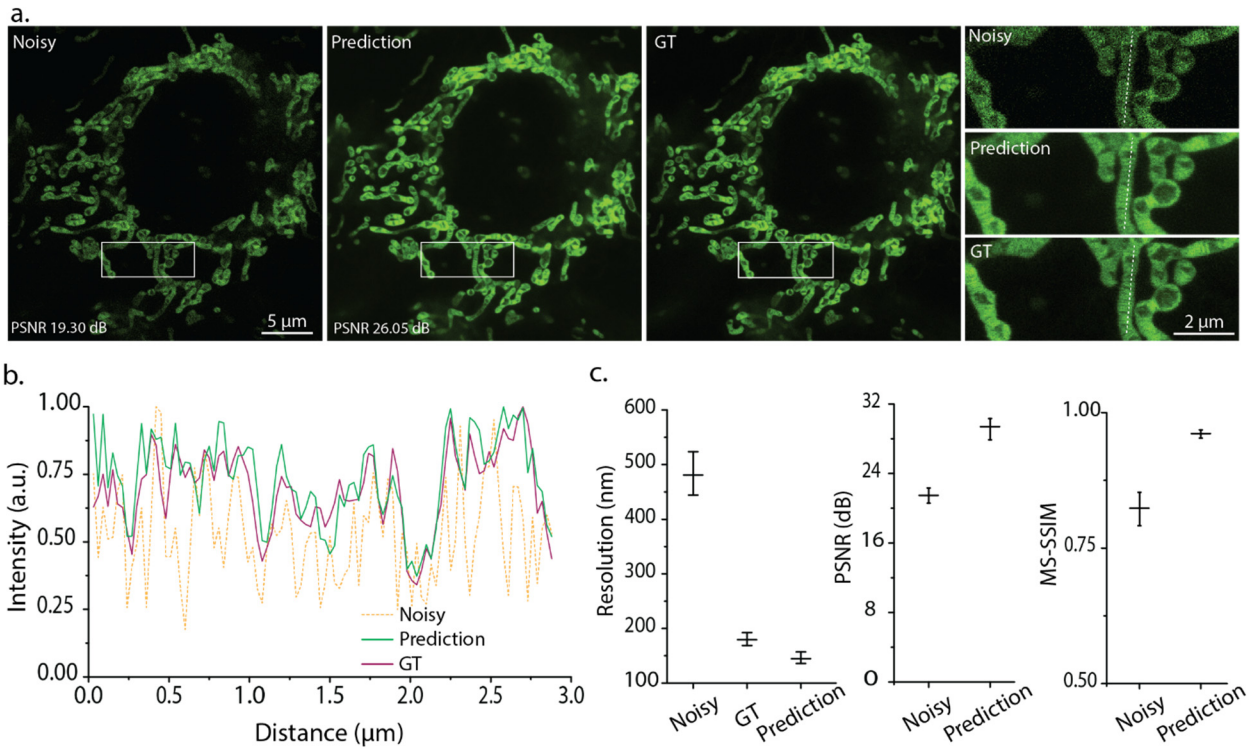

Supplementary Fig. 2, Denoising performance of UNet-RCAN on the semi-synthetic dataset. (a) Denoising results of cristae labeled with PK Mito Orange in HeLa cells. The GT data was captured with a dwelling time of 90 µs. The noisy data was generated by adding Poisson noise. The prediction is the denoising result by UNet-RCAN. (b) Line profiles of noisy, prediction, and GT data along the dashed lines in (a). (c) Resolution analysis by decorrelation, PSNR, and MS-SSIM calculations were performed on the prediction results by UNet-RCAN. Mean and standard deviation are displayed (*n* = 10).

Supplementary Note 1, Comparisons with other deep learning approaches

In cross-modality image restoration, a diffraction-limited confocal image is transformed into a super-resolved STED image with resolution enhancement by a deep convolutional neural network[1]. Different network architectures could perform this image transformation, such as generative adversarial networks (GAN)[2] or residual channel attention networks (RCAN)[3]. A transformation between confocal and STED imaging modalities at least requires a 3~5-fold resolution enhancement, i.e., from 250 nm to 50 nm; however, the cross-modality deep learning approaches have proven to be limited by a factor of 2-2.5 in terms of resolution enhancement[3]. Moreover, a lack of enough information often leads to exhibit artifacts.

Unlike the cross-modality image transformation, denoising is performed on noisy but super-resolved STED images to improve SNR. In denoising, the input data contains more information in terms of spatial resolution. This can help to reduce artifact generation and improve resolution enhancement. In Figs.1f-h, we showed that denoising STED data clearly outperforms the cross-modality approach perceptually and according to the image quality assessment parameters.

Two popular network architectures suitable for denoising super-resolution data are UNet and RCAN. A UNet learns the features in an image dataset through convolutional layers and multiple down-sampling and up-sampling layers. Although the UNet effectively denoises diffraction-limited imaging data such as widefield images, its output does not reliably preserve high-frequency information. This is likely due to the fact that there is no mechanism to prioritize high-frequency information. Moreover, in UNet, a final image is reconstructed through downsampling and upsampling layers rather than applying the convolutional filters on the original noisy super-resolved data.

On the other hand, RCAN contains channel attention blocks and several skip connections, which help prioritize and maintain high-frequency information in super-resolution image reconstruction. Moreover, in RCAN, final super-resolved images are restored by applying filters on the original noisy data. This lowers the possibility of missing high-frequency information. However, our STED denoising results with RCAN show that although its final result is superior to UNet in terms of resolution, it generates more high-frequency artifacts, which may be due to its CAB building blocks, especially when the input SNR is extremely poor.

We showed that by combining UNet and RCAN, denoising could be effectively performed on fast STED data while we can maintain the super-resolution and prevent high-frequency artifact generation.

Supplementary Tables

Supplementary Table 1. Parameters and training time for CARE, 2D-RCAN, and UNet-RCAN.

	CARE	2D-RCAN	UNet-RCAN
# Iterations per epoch	70	1,080	1,080
Batch size	16	1	1
Patch size	256×256	256×256	256×256
Epochs	200	200	200
Number of parameters	3,790,850	3,944,073	16,684,270
Training time	1 h 17 m	11 h 40 m	8 h 10 m

Supplementary Table 2. Performance comparison chart of UNet-RCAN, CARE, and 2D-RCAN in terms of SNR.

	Noisy	CARE	2D-RCAN	UNet-RCAN
β-tubulin	21.3±1.1 dB	23.0±1.6 dB	22.0±1.6 dB	27.2±1.3 dB
Clathrin	26.2±1.1 dB	27.4±3.0 dB	25.6±1.2 dB	29.3±1.1 dB
Histone	16.2±0.6 dB	20.4±0.8 dB	21.2±0.8 dB	21.6±0.9 dB
TOM20	18.0±0.7 dB	23.1±1.3 dB	20.9±0.8 dB	24.6±0.6 dB
Vimentin	17.7±0.9 dB	23.0±1.8 dB	23.0±1.1 dB	24.2±1.1 dB

Supplementary Table 3. Performance comparison chart of UNet-RCAN, CARE, and 2D-RCAN in terms of similarity.

	Noisy	CARE	2D-RCAN	UNet-RCAN
β-tubulin	0.61±0.04	0.77±0.05	0.73±0.06	0.83±0.02
Clathrin	0.79±0.03	0.87±0.03	0.83±0.03	0.88±0.02
Histone	0.53±0.06	0.67±0.04	0.66±0.04	0.70±0.06
TOM20	0.59±0.03	0.79±0.02	0.80±0.01	0.81±0.02
Vimentin	0.58±0.05	0.81±0.05	0.83±0.04	0.85±0.06

Supplementary Table 4. Performance comparison chart of UNet-RCAN, CARE, and 2D-RCAN in terms of resolution measured by decorrelation analysis.

	CARE	2D-RCAN	UNet-RCAN
β-tubulin	80±3 nm	71±3 nm	51±1 nm
Clathrin	122±5 nm	103±6 nm	81±4 nm
Histone	166±2 nm	115±2 nm	110±1 nm
TOM20	193±2 nm	179±3 nm	98±2 nm
Vimentin	243±1 nm	115±13 nm	101±1 nm

Supplementary Table 5. Acquisition settings of STED imaging.

Figures		
1b, 2a ED 2a,4a,5, 9	Exc. power = 20% STED power = 50% Resonant scanning Gating: 0.4-12 ns Leica STED	Fluorophore: STAR635P, λ_{exc} = 635 nm, λ_{STED} = 775 nm Pixel time: 0.054 μs (noisy) and 2.3 μs (ground-truth)
2a		Fluorophore: Alexa 594, λ_{exc} = 594 nm, λ_{STED} = 775 nm Pixel time: 0.054 μs (noisy) and 2.3 μs (ground-truth)
ED 10a		Fluorophore: STAR635P, λ_{exc} = 635 nm, λ_{STED} = 775 nm Pixel time: 0.025 μs (noisy) and 1μs (ground-truth)
1f ED 3a, 4b, 4c, 8a, 8b		Fluorophore: Atto647N, λ_{exc} = 647 nm, λ_{STED} = 775 nm Pixel time: 0.054 μs (noisy) and 2.3 μs (ground-truth)
ED 3b		Fluorophore: Atto647N, λ_{exc} = 647 nm, λ_{STED} = 775 nm Pixel time: 0.090 μs (noisy) and 2.3 μs (ground-truth)
ED 5, 8a, 9		Fluorophore: STAR580, λ_{exc} = 580 nm, λ_{STED} = 775 nm Pixel time: 0.054 μs (noisy) and 2.3 μs (ground-truth)
ED 7a, 7c		Fluorophore: Atto647N, λ_{exc} = 647 nm, λ_{STED} = 775 nm Pixel time: [0.018,0.036,0.072,0.108,0.144] μs (noisy) and 2.3 μs (ground-truth)
ED 7a, 7c		Fluorophore: STAR580, λ_{exc} = 580 nm, λ_{STED} = 775 nm Pixel time: [0.018,0.036,0.072,0.108,0.144] μs (noisy) and 2.3 μs (ground-truth)
ED 6a	Exc. power = 20% STED power = [0%,10%,20%,50%,70%], Resonant scanning Gating: 0.4-12 ns Leica STED	Fluorophore: STAR635P, λ_{exc} = 635 nm, λ_{STED} = 775 nm Pixel time: 0.050 μs (noisy) and 1.0 μs (ground-truth)
2g, ED 10b	Exc. power = 20% 2D-STED power = 50% z-STED power = 50% Resonant scanning Gating: 0.4-12 ns	Fluorophore: Atto647N, λ_{exc} = 635 nm. λ_{STED} = 775 nm Pixel time: 0.018 μs (noisy) and 2.3 μs (ground-truth)

	Leica STED	
2c, 2d SI 2a	Exc. power = 4.5% STED power = 22% Galvo scanning Gating: 0.75-8 ns Abberior STED	Fluorophore: PK Mito Orange, λ_{exc} = 561 nm, λ_{STED} = 775 nm Pixel time: 1 μs (noisy)
2h	Exc. power = 35% 2D-STED power = 0% z-STED power = 100% Galvo scanning Gating: 0 ns Abberior STED	Fluorophore: NR4A , λ_{exc} = 561 nm, λ_{STED} = 775 nm Pixel time: 2 μs (noisy) and 20 μs (ground-truth)

Supplementary Table 6. Immunolabeling conditions.

Figures	Primary antibody	Secondary antibody	Fluorophore
1b, 2a ED 2a, 5, 6a, 9	Monoclonal Anti-β-Tubulin antibody produced in mouse, Sigma-Aldrich, T5293	Fab Fragment Goat Anti-Mouse IgG1, Jackson ImmunoResearch, 115-007-185	Abberior STAR 635P
ED 7a, 7c, 8a	Monoclonal Anti-β-Tubulin antibody produced in mouse, Sigma-Aldrich, T5293	Fab Fragment Goat Anti-Mouse IgG1, Jackson ImmunoResearch, 115-007-185	Abberior STAR 580
ED 5, 9	Anti-Clathrin heavy chain antibody (ab21679)	Fab Fragment Goat Anti-Rabbit IgG, Jackson ImmunoResearch, 111-007-008	Abberior STAR 580
1f ED 4b, 7a, 7c, 8a, SI 4a	Anti-acetyl-Histone H3 (Lys9) in rabbit, Sigma-Aldrich, 07-352	Rabbit IgG (H&L) Antibody ATTO 647N Conjugated Pre-Adsorbed, ROCKLAND, 611-156-122	Atto 647N
2a	Anti-acetyl-Histone H3 (Lys9) in rabbit, Sigma-Aldrich, 07-352	Alexa Fluor® 594 AffiniPure $F(ab')_2$ Fragment Goat Anti-Rabbit IgG (H+L)	Alexa Fluor 594
2g ED 3a, 3b, 4c, 10b	Anti-TOMM20 antibody - Mitochondrial Marker, abcam, ab78547	Rabbit IgG (H&L) Antibody ATTO 647N Conjugated Pre-Adsorbed, ROCKLAND, 611-156-122	Atto 647N

ED 4a	Anti-Vimentin antibody, Mouse monoclonal (V6389-200UL)	Fab Fragment Goat Anti-Mouse IgG1, Jackson ImmunoResearch, 115-007-185	Abberior STAR 635P

References

1. Wang, H.D. et al. Deep learning enables cross-modality super-resolution in fluorescence microscopy. *Nat Methods* **16**, 103-110 (2019).
2. Speiser, A. et al. Deep learning enables fast and dense single-molecule localization with high accuracy. *Nat Methods* **18**, 1082-1090 (2021).
3. Chen, J.J. et al. Three-dimensional residual channel attention networks denoise and sharpen fluorescence microscopy image volumes. *Nat Methods* **18**, 678-687 (2021).